

Electron and hole relaxation pathways in semiconductor quantum dots

V. I. Klimov* and D. W. McBranch

Chemical Sciences and Technology Division, CST-6, MS-J585, Los Alamos National Laboratory, Los Alamos, New Mexico 87545

C. A. Leatherdale and M. G. Bawendi

Department of Chemistry and Center for Materials Science and Engineering, Massachusetts Institute of Technology, 77 Massachusetts Avenue, Cambridge, Massachusetts 02139

(Received 15 March 1999)

Femtosecond (fs) broad-band transient absorption (TA) is used to study the intraband relaxation and depopulation dynamics of electron and hole quantized states in CdSe nanocrystals (NC's) with a range of surface properties. Instead of the drastic reduction in the energy relaxation rate expected due to a "phonon bottleneck," we observe a fast subpicosecond $1P$ -to- $1S$ electron relaxation, with the rate exceeding that due to phonon emission in bulk semiconductors. The energy relaxation is enhanced with reducing the NC's radius, and does not show any dependence on the NC surface properties (quality of the surface passivation). These data indicate that electron energy relaxation occurs by neither multiphonon emission nor by coupling to surface defects, but is likely mediated by Auger-type electron-hole energy transfer. We use fs infrared TA to probe electron and hole intraband transitions, which allows us to distinguish between electron and hole relaxation pathways leading to the depopulation of NC quantized states. In contrast to the electron relaxation, which is controlled by NC surface passivation, the depopulation of hole quantized states is extremely fast (sub-ps-to-ps time scales) in all types of samples, independent of NC surface treatment (including NC's overcoated with a ZnS layer). Our results indicate that ultrafast hole dynamics are not due to trapping at localized surface defects such as a vacancy, but rather arise from relaxation into intrinsic NC states or intrinsically unpassivated interface states. [S0163-1829(99)02843-X]

I. INTRODUCTION

Semiconductor nanocrystals (NC's), also referred to as semiconductor quantum dots (QD's), represent a class of quantum-confined objects in which carrier motion is restricted in all three dimensions (3D). 3D quantum confinement results in discrete size-dependent electron and hole energy spectra. In spherical QD's, carrier energies increase with reducing NC radius (R) roughly as R^{-2} .^{1,2} Epitaxial techniques such as Stranski-Krastanov growth,³ have been widely applied to the preparation of self-assembled III-V QD's. However, epitaxially-grown QD's have relatively large lateral sizes (>10 nm) which do not allow one to investigate the interesting regime of very strong confinement for which the energy level spacing greatly exceeds both the bulk-exciton binding energy and the energies of longitudinal-optical (LO) phonons. An alternative approach to making high quality 3D-confined nanostructures utilizes chemical synthesis, based on the control of homogeneous nucleation, which allows preparation of NC's in the 1–10 nm size regime. Such chemical methods are particularly well developed for II-VI QD's. There are two main chemical routes for preparation of II-VI NC's: high-temperature inorganic precipitation in molten glasses^{4,5} and colloidal synthesis using, e.g., organometallic reactions.^{6,7} Glass samples provide rigidity and environmental stability, but they have a broad NC size distribution (typically greater than 15%) and a large amount of surface defects. A much higher level of synthetic flexibility and control is provided by colloidal NC's which can be chemically manipulated in a variety of ways including size-selective techniques⁷ (resulting in less than 5% size

variations), surface modification by exchanging the passivation layer,⁸ heterostructure with formation of layered NC's,⁹ immobilization in sol-gel¹⁰ and polymer¹¹ matrices, and self-assembly into 3D superlattices.¹²

Due to the discrete structure of energy levels and an enhanced surface-to-volume ratio, energy relaxation and recombination dynamics in NC's are significantly different from those in bulk materials. In bulk II-VI semiconductors, carrier energy relaxation is dominated by the Fröhlich interaction with LO phonons, leading to fast (typically sub-ps) carrier cooling dynamics.^{13–15} In NC's, even in the regime of weak confinement when the level spacing is only a few meV, the carrier relaxation mediated by interactions with phonons is hindered dramatically, because of restrictions imposed by energy and momentum conservation leading to a phenomenon called a "phonon bottleneck."^{16,17} Further reduction in the energy loss-rate is expected in the regime of strong confinement, for which the level spacing can be much greater than LO phonon energies, and hence carrier-phonon scattering can only occur via weak multi-phonon processes. Calculations performed for GaAs QD's (Ref. 18) show that the energy-loss rate for two-phonon emission is orders of magnitude lower than for a single-phonon process, and is further reduced with increasing a number of phonons participating in the process.

Despite these theoretical predictions, a number of recent experimental results indicate that carrier relaxation in II-VI NC's is not significantly slower than in bulk materials. Such evidence includes a lack of hot-carrier emission in femtosecond (fs) photoluminescence (PL) studies,¹⁹ a fast build-up of the nonlinear signal in transient absorption (TA)

experiments,²⁰ sub-picosecond (sub-ps) relaxation of TA features associated with Coulomb two-pair interactions,²¹ and a fast build-up of $1S$ - $1P$ intraband absorption.²² Strong evidence against the existence of the phonon-bottleneck in strongly confined QD's has been obtained in recent studies of intraband electron relaxation in CdSe NC's (Ref. 23) which indicate sub-ps $1P$ -to- $1S$ electron relaxation even in NC's for which $1S$ - $1P$ energy separation is as high as ~ 16 LO phonon energies. Similar results indicating extremely fast electron intraband relaxation have been recently reported for III-V QD's.²⁴

Energy relaxation leads to the establishment of quasiequilibrium populations of electron and hole quantized states. Depopulation of these states can occur via a variety of radiative and non-radiative mechanisms. The radiative electron-hole (e - h) recombination in CdSe NC's is a relatively slow process with ns time constants.²⁵ Competing deactivation mechanisms are non-radiative (phonon-assisted) e - h recombination, carrier trapping at defect/surface states,^{19,23,26} and Auger recombination,^{27,28} with the latter dominating carrier dynamics in the regime of multiple e - h pair excitations. Carrier dynamics in NC's have been studied using fs TA,^{20,23,26} PL,¹⁹ and four-wave mixing^{29,30} experiments. The fast initial dynamics observed in these experiments have been usually explained in terms of carrier trapping at defect sites (often presumed surface-related). However, the mechanisms for carrier trapping and the origin of trapping sites have not been understood yet. Additionally, most ultrafast studies of II-VI quantum dots have concentrated on NC/glass samples which have poorly-controlled surface properties. Therefore, it remains unclear whether the fast initial depopulation of quantized states in NC's is entirely due to trapping at surface defects or due to relaxation into intrinsic quantum dot states.

Recently, we reported energy relaxation studies in CdSe NC's with emphasis on glass samples.²³ In the present paper, we study well-characterized CdSe colloidal samples to investigate in detail the effect of quantum confinement and surface properties on energy relaxation dynamics. In agreement with previous results for glass samples, we observe a shortening of the population time of the lowest $1S$ electron state with reducing the NC radius, which follows roughly a linear size dependence. We find that the $1S$ -state population dynamics are nearly identical in colloids with different surface passivations, indicating a negligible role of surface defects in the electron intraband relaxation. In addition to studies of intraband relaxation, we report studies of carrier dynamics during the subsequent stage of depopulation of NC quantized states. We observe that the initial decay of the $1S$ -electron population is strongly dependent on degree of surface passivation, suggesting that it is due to trapping at surface defects. To study hole relaxation dynamics, we use infrared (IR) TA spectroscopy of intra-band transitions. In contrast to electron dynamics, controlled by NC surface passivation, hole dynamics are nearly identical and extremely fast (sub-ps-ps time scales) in samples with different surface properties, suggesting that these dynamics are not due to trapping at surface defects such as vacancies but rather are due to relaxation into intrinsic NC states, or surface states that remain unpassivated even under the range at surface treatments of this work.

II. EXPERIMENT

To probe carrier relaxation dynamics, we monitored carrier-induced absorption changes using high-sensitivity fs TA experiment in the pump-probe configuration. Samples were pumped at 3 eV by frequency-doubled 100-fs pulses from an amplified Ti-sapphire laser. In the visible TA measurements, the transmission of the photoexcited spot was probed by variably delayed pulses of a white-light fs continuum. TA spectra were detected in the chirp-free mode³¹ with an accuracy up to 10^{-5} in differential transmission. In IR TA measurements, the probe pulses were derived from an IR optical parametric amplifier, tunable in the range 1.1–2.7 μm . IR signals were detected with liquid- N_2 -cooled HgCdTe photodetectors.

We studied CdSe NC's prepared by colloidal synthesis⁷ and high-temperature precipitation in molten glasses.⁴ Colloidal CdSe samples were of two types: NC's passivated with molecules of tri- n -octylphosphine oxide⁷ (TOPO) and "overcoated" NC's, surrounded by a final layer of ZnS,³² (both dissolved in hexane). NC sizes and size distributions were determined from linear absorption spectra using calibration curves derived from comparison of optical data with data of transmission electron microscopy and small-angle x-ray scattering.⁷ The NC mean radii varied from ~ 1 to ~ 4 nm. The NC size dispersion was 4–9% in colloids and 15–25% in glass samples. All measurements were performed at room temperature.

To exclude effects of many-particle interactions on carrier dynamics, the relaxation data were taken at low pump intensities corresponding to $N_{eh} < 1$ (unless otherwise is stated), where N_{eh} is the average number of e - h pairs excited per NC. N_{eh} can be computed as $N_{eh} = j_p \sigma_a$, where j_p is the pump fluence (presented in photons per cm^2) and σ_a is the NC absorption cross section. In the case of pumping high above the NC energy gap, the NC absorption cross section can be calculated using the expression $\sigma_a = (4\pi/3)|f|^2 \alpha_b R^3$, where α_b is the bulk absorption coefficient at the pump wavelength, and f is a coefficient accounting for local-field effects.³³ Using $\alpha_b = 1.6 \times 10^5 \text{ cm}^{-1}$ and $|f|^2 = 0.25$ (both at $\hbar\omega = 3 \text{ eV}$), we find that for the CdSe NC's studied (radius from ~ 1 to ~ 4 nm) the NC absorption cross sections are in the range $\sim (0.2\text{--}10) \times 10^{-15} \text{ cm}^2$.

III. ELECTRON ENERGY RELAXATION DYNAMICS

In Fig. 1, we show linear absorption spectra of a series of TOPO-passivated colloidal NC's with mean radii from 1.17 to 4.05 nm. Due to the narrow NC size distribution, the absorption spectra clearly exhibit discrete features due to transitions coupling electron and hole quantized states. It has been shown using PL-excitation studies³⁴ that these features can be explained by effective-mass theory, taking into account confinement-induced mixing of three valence subbands.³⁵ In this theory, electron states are labeled using a letter (l) to denote the angular momentum of the envelop wave function [S for $l=0$, P for $l=1$, D for $l=2$, etc.] and a digit to denote a number of the state of the given symmetry. The three lowest electron states in the order of increasing energy are $1S$, $1P$, $1D$. A similar notation is used for hole states with an addition of a subscript which denotes the total

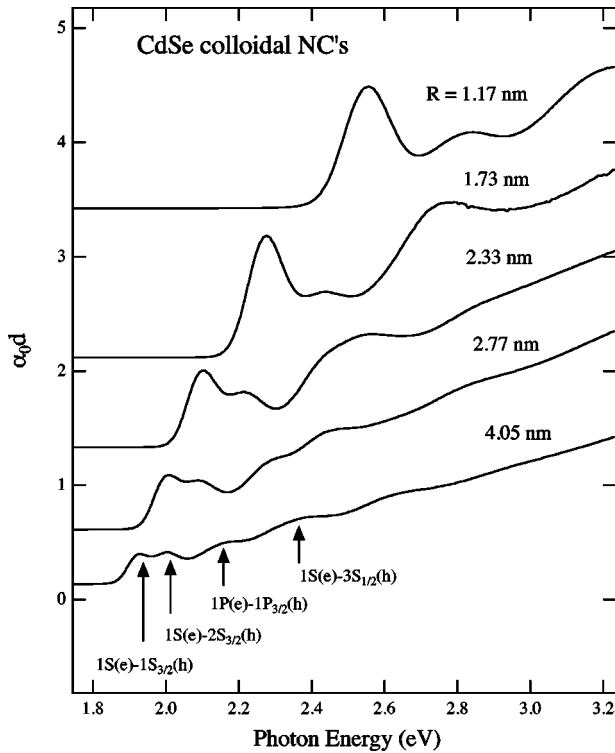


FIG. 1. Linear absorption spectra of TOPO-passivated CdSe NC's (radii from 1.17 to 4.05 nm).

hole angular momentum, which is the sum of the valence-band Bloch-function momentum and the momentum of the hole envelope wave function. In CdSe NCs with $R > 2$ nm, first three hole states in the order of increasing energy are $1S_{3/2}$, $1P_{3/2}$, $2S_{3/2}$.³⁵

The two lowest bands in the linear absorption spectra of Fig. 1 can be assigned to transitions involving the lowest electron state ($1S$) and two different hole states ($1S_{3/2}$ and $2S_{3/2}$). In the following, we will refer to these transitions as $1S$ [$1S(e)-1S_{3/2}(h)$] and $2S$ [$1S(e)-2S_{3/2}(h)$]. The linear absorption spectra of NC's with $R > 2.3$ nm also exhibit a well-resolved band associated with the transition coupling the $1P$ electron state to the $1P_{3/2}$ hole state ($1P$ transition) and a higher-lying band associated with the transition involving the $1S$ electron state and a hole state originating from the spin-orbit split-off band ($3S_{1/2}$ for NC with $R = 4.05$ nm; see Fig. 1).

In Fig. 2, we present early-time TA spectra (the pump-probe delay time $\Delta t = 200$ fs) recorded for the same series of NC's as shown in Fig. 1. The nonlinear optical response in NC's is dominated by state-filling^{20,23} leading to pronounced bleaching bands at energies of allowed optical transitions. Comparison of TA data (Fig. 2) with linear absorption spectra (Fig. 1) allows us to assign TA bleaching features B_1 , B_2 , and B_3 to the $1S$, $2S$, and $1P$ transitions, respectively. In addition to state filling, the TA of NC's is also affected by Coulomb many-particle interactions (e.g., the biexciton effect^{21,36,37} and a trapped-carrier-induced dc Stark effect³⁸), leading to a shift of optical transitions with associated photoinduced-absorption (PA) features at the positions of the shifted transitions. Such PA features can be discerned below the $1S$ (A_1) and $1P$ (A_2) transitions (Fig. 2).

The magnitude of the state-filling-induced bleaching is

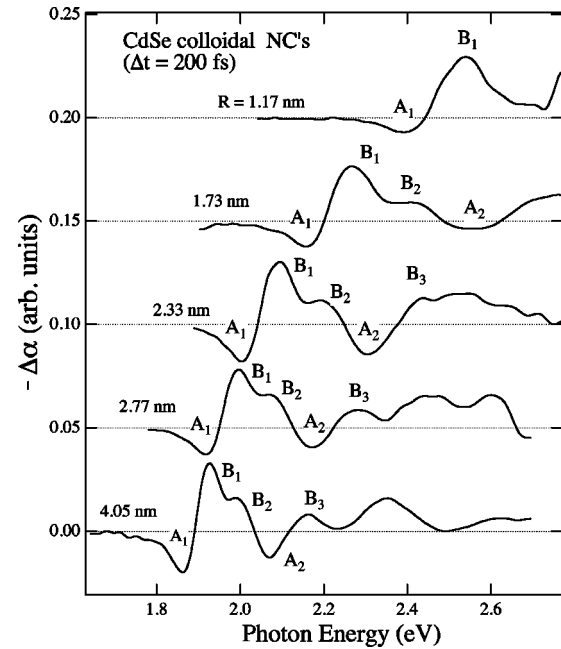


FIG. 2. TA spectra of TOPO-passivated CdSe NC's (radii from 1.17 to 4.05 nm) recorded 200 fs after excitation.

proportional to the sum of occupation numbers of the quantized electron and hole states involved in the transition. However, due to degeneracy of the valence band, and the large difference between electron and hole masses ($m_h/m_e \approx 6$), the room-temperature occupation probability of the lowest electron state is much greater than that of the coupled hole state (the hole population is spread over many adjacent levels by the thermal distribution). As a result, the state-filling-induced portion of TA is dominated by the electrons.³⁹ This is clearly indicated by the fact that in both colloidal and glass samples, the $1S$ and $2S$ bleaching bands, which involve the same electron ($1S$) but different hole

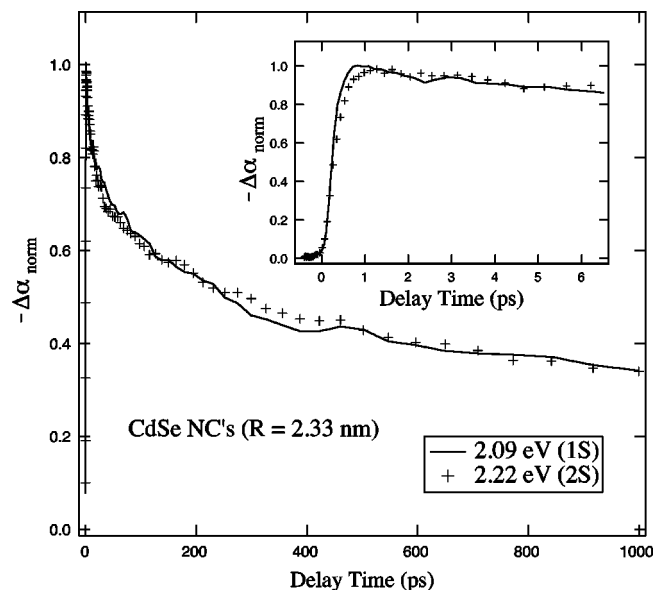


FIG. 3. Nanosecond (mainframe) and picosecond (inset) TA dynamics at the positions of the $1S$ (solid line) and $2S$ (crosses) transitions (TOPO-passivated CdSe NC's with $R = 2.33$ nm).

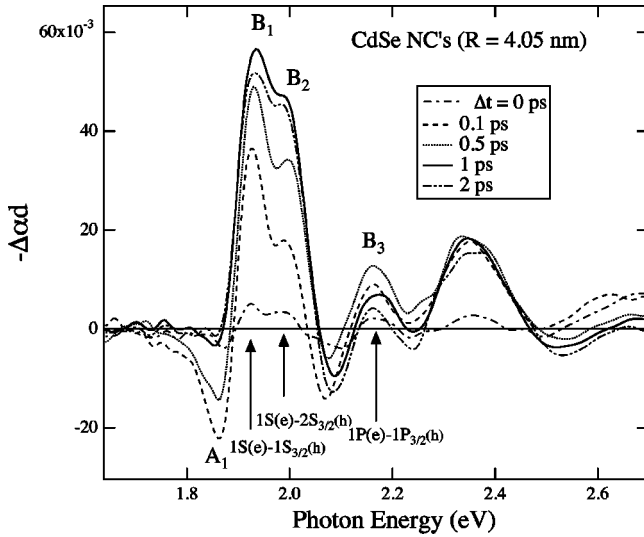


FIG. 4. Chirp-free TA spectra for TOPO-passivated CdSe NC's ($R=4.05$ nm) recorded at different delay times between pump and probe pulses.

states, show essentially identical dynamics at $\Delta t > 2-3$ ps (after the intraband energy relaxation is finished); both signals are dominated by the depopulation dynamics of the common $1S$ electron level. To illustrate this result, in Fig. 3, we show the exactly matching $1S$ and $2S$ TA dynamics recorded for a TOPO-passivated colloidal sample with $R = 2.33$ nm over both ps (inset) and ns (main frame) time scales.

In our studies of energy relaxation, we concentrate on the population re-distribution between adjacent $1P$ and $1S$ electron states. In Fig. 4, we show chirp-free TA spectra of TOPO-passivated NC's with $R = 4.05$ nm recorded between 0 and 2 ps after excitation. For this NC size the $1S-1P$ energy separation is about eight LO phonon energies. On the time scale shown in Fig. 4, TA dynamics are dominated by the intraband energy relaxation. Interestingly, a nonzero TA response over the whole spectral range ($\sim 1.7-2.7$ eV) is observed already at $\Delta t = 0$. This is a result of the Coulomb two-pair interaction (biexciton effect),^{21,36,37} leading to the instantaneous shift of all optical transitions in the presence of the $e-h$ pair excited by the pump pulse. The shift of the $1S$ transition induced by the two $e-h$ pair interaction is seen in early-time TA spectra ($\Delta t < 0.5$ ps) as a derivative-like feature with bleaching at 1.93 eV (B_1) and induced absorption (A_1) at 1.86 eV. With increasing pump-probe delay time, A_1 rapidly decays, whereas B_1 grows due to increasing population of the $1S$ electron state as a result of energy relaxation from higher states. The B_1 growth is accompanied by the decay of the B_3 band associated with the $1P$ transition.

Very illustrative are time transients recorded at the positions of the $1S$ and $1P$ transitions (Fig. 5). For the 4.05 -nm sample [Fig. 5(a)], the B_3 feature decays with a 540 -fs time constant, which we attribute to the depopulation of the $1P$ state. The B_1 time transient shows a fast initial rise due to the biexciton effect, followed by a slower signal increase with a 530 -fs time constant. The secondary B_1 growth is complementary to the B_3 decay and is associated with increasing $1S$ population, due to the $1P$ -to- $1S$ relaxation. It is also quite interesting to examine $1P$ relaxation as a function of excita-

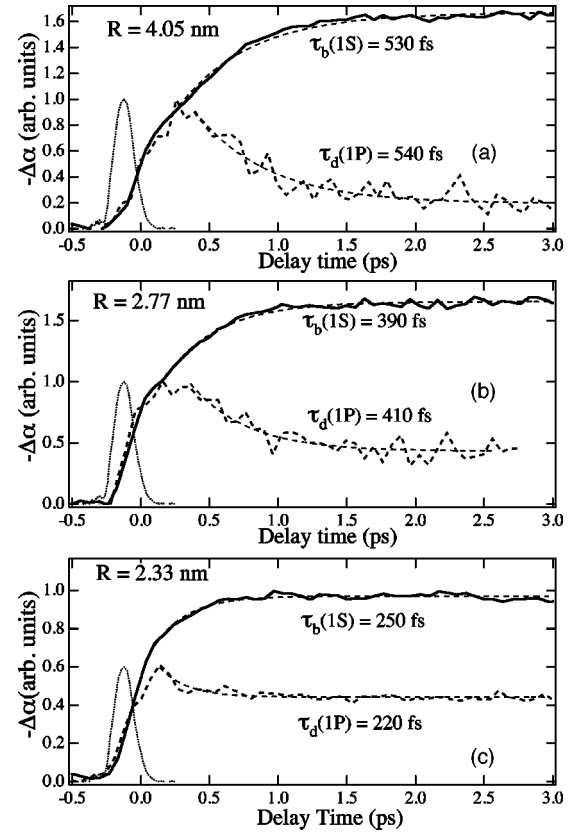


FIG. 5. TA dynamics recorded at the positions of the $1S$ (thick solid line) and the $1P$ (thick dashed line) transitions for TOPO-passivated CdSe NC's with $R = 4.05$ nm (a), 2.77 nm (b), and 2.33 nm (c). Thin dotted line is a pump-probe cross-correlation. Thin dashed lines are fits to a single-exponential decay (build-up) (τ_d and τ_b are corresponding time constants).

tion density (Fig. 6). With increasing the pump level, the decay of the B_3 feature becomes slower, indicating the saturation of the final state at the bottom of the conduction band. The saturation occurs at pump intensities corresponding to $N_{eh} = 1-2$, as expected for a two-fold degenerate $1S$ electron state. This result provides additional evidence that the

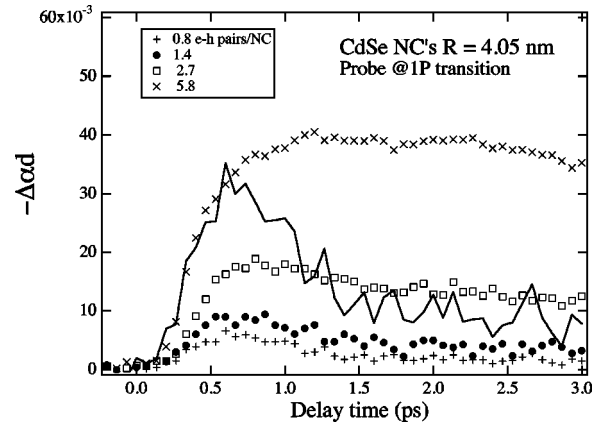


FIG. 6. Short-term TA dynamics (symbols) at the position of the $1P$ transition in TOPO-passivated CdSe NC's ($R = 4.05$ nm) as a function of excitation density [number of $e-h$ pairs (N_{eh}) per NC]. Line is a scaled time transient recorded at the lowest pump level ($N_{eh} = 0.8$).

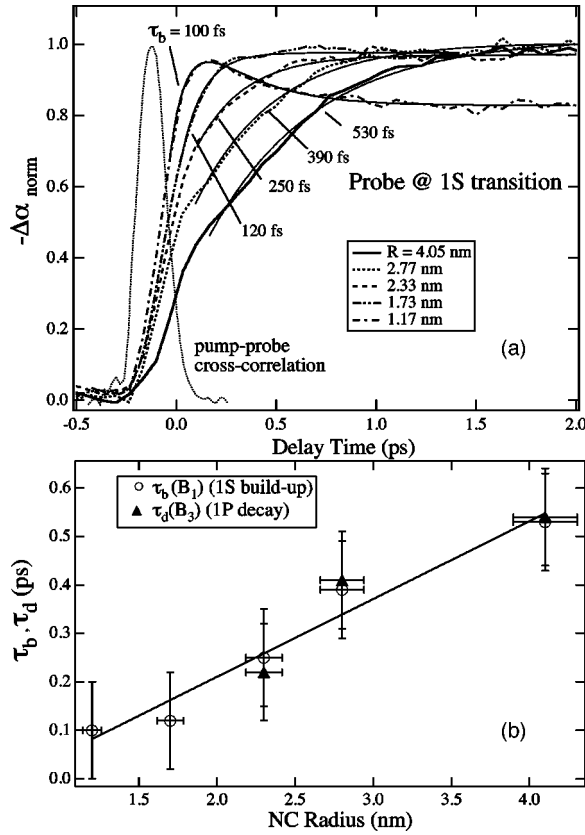


FIG. 7. (a) The 1S bleaching build-up dynamics for TOPO-passivated CdSe NC's of different size (thick lines) fit to a single-exponential growth (thin solid lines). Thin dotted line is a pump-probe cross correlation. (b) The dependence of the 1P-decay (triangles) and the 1S build-up (circles) times on the NC radii, fit to a linear size dependence (line).

observed dynamics are due to direct electron relaxation into the lowest 1S state.

Complementary 1S and 1P dynamics are also observed for NC's with radii of 2.77 and 2.33 nm [Fig. 5(b) and 5(c), respectively]. For the smaller NC's, the 1P decay becomes less pronounced due to increasing overlap of the 1P transition with the nearby 1S(e)-2S_{1/2}(h) transition. In contrast to predictions of phonon-bottleneck theories,^{17,18} the 1P-to-1S relaxation becomes faster with reducing NC radius. For 2.77-nm NC's, the relaxation time is around 400 fs, and further shortens down to \sim 220 fs in NC's with $R=2.33$ nm. The important role of spatial confinement in the enhancement of the energy relaxation is evident from a comparison of the 1S state population dynamics in NC's of different radii [see Fig. 7(a)], indicating a decrease in the 1S build-up time with decreasing NC radius. This time shortens from 530 fs for $R=4.05$ nm to 100 fs for $R=1.17$ nm, roughly following a linear dependence [Fig. 7(b)].

It is illustrative to compare the rate of energy relaxation observed in NC's with that in bulk materials. Carrier energy losses in bulk CdSe are dominated by the Fröhlich interaction with LO phonons.^{14,15} In the case of a negligible role of screening of the electron-phonon interaction⁴⁰ and non-equilibrium filling of phonon modes^{15,41} (both effects reduce the efficiency of carrier cooling), the electron energy loss for the Fröhlich mechanism can be estimated from the following expression [we assume that the electron energy is much

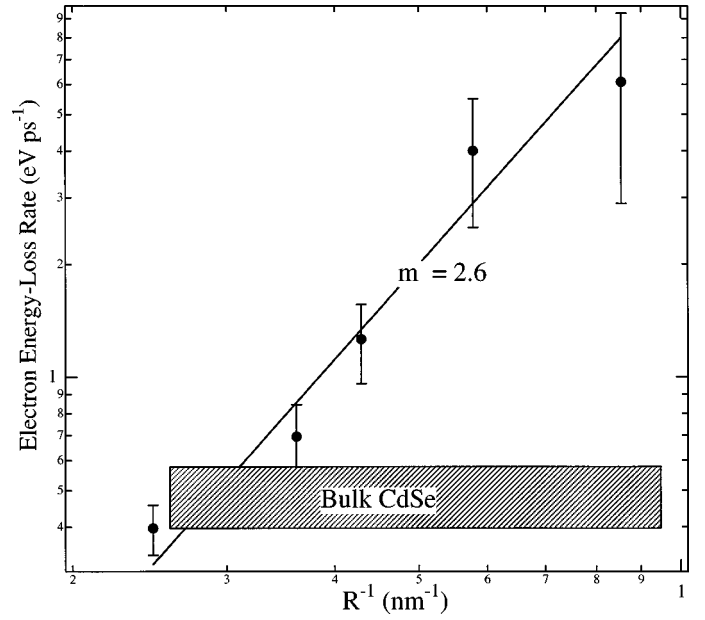


FIG. 8. Size dependence of the electron energy-loss rate in CdSe NC's (symbols) fit to a function $(dE_e/dt) \propto R^{-2.6}$ (line). The shaded region shows the range of energy-loss rates characteristic of electron-LO-phonon scattering in bulk CdSe.

greater than the LO-phonon energy ($\hbar\omega_0$)]:¹³

$$\frac{dE_e}{dt} = -\beta\hbar\omega_0^2 \left(\frac{\hbar\omega_0}{E_e}\right)^{1/2} \ln\left(\frac{4E_e}{\hbar\omega_0}\right), \quad (3.1)$$

where β is a polar-interaction constant (in CdSe, $\beta=0.46$) and E_e is the electron energy measured from the bottom of the conduction band. For electron energies corresponding to the 1S-1P energy spacing in NC's of sizes studied, the bulk-CdSe energy-loss rate is in the range ~ 0.4 – 0.6 eV ps⁻¹ (shaded region in Fig. 8).

The energy-loss rate for NC's can be estimated from the ratio of the 1S-1P energy separation (ΔE_{sp}) and the time of the 1P-to-1S relaxation. For 4.05-nm NC's, this gives the rate of ~ 0.4 eV ps⁻¹, which is essentially the same as in bulk materials, but many orders of magnitude greater than the rate expected for a multi-phonon emission¹⁸ (in 4.05-nm NC's the 1S-1P energy separation is around $8\hbar\omega_0$). The energy-loss rate rapidly increases with reducing NC size (Fig. 8). For the smallest size studied ($R=1.17$ nm; $\Delta E_{sp} = 23\hbar\omega_0$), it is ~ 6 eV ps⁻¹, which is an order of magnitude greater than for LO phonon emission in bulk materials. The experimental data in Fig. 8 can be well fit to the dependence $(dE_e/dt) \propto R^{-2.6}$, indicating a strong confinement-induced enhancement in the energy relaxation rate which is approximately inversely proportional to the NC volume. This trend is exactly the opposite to that expected for phonon-mediated relaxation, for which the relaxation rate slows down with reducing the NC size because of the increasing numbers of phonons required to dissipate each quantized electron jump.

Extremely fast electron relaxation, as well as a confinement-induced enhancement in the relaxation process, clearly indicate that energy relaxation in NC's is dominated by *non-phonon* energy-loss mechanisms. Recent works have suggested that coupling to defects⁴² and/or Auger-type

interactions^{43,44} can lead to fast energy relaxation not limited by a phonon bottleneck. The first of these mechanisms suggests a sequential relaxation involving an electron transition to the defect (associated, e.g., with a surface dangling bond), defect relaxation, and then transition back to the lower NC level. This scenario is obviously not consistent with the measured complementary dynamics of the $1P$ and $1S$ states (Fig. 5), indicating a direct $1P$ -to- $1S$ electron transition. The negligible role of defect states is also indicated by comparison of energy-relaxation data for TOPO- and ZnS-capped samples. Overcoating NC's with ZnS significantly reduces the number of surface defects, as indicated by the slowing down of the $1S$ bleaching decay (see the next section). However, this improvement in surface passivation does not lead to any significant changes in the $1S$ build-up dynamics, indicating that the energy relaxation rate is not affected by the number of surface defects.

The Auger-type mechanism analyzed in Ref. 43 involves energy transfer from the electron to high density $e-h$ plasmas (2D plasmas from the adjacent quantum well in Ref. 43). However, this effect cannot be operative under our experimental conditions of low excitation densities (less than 1 $e-h$ pair per NC) and with NC's dispersed in an insulating, optically transparent host. The observed fast dynamics are best explained in terms of the Auger mechanism proposed in Ref. 44 which involves confinement-enhanced energy transfer of the electron excess energy to a hole, with subsequent fast hole relaxation through its dense spectrum of states. According to the estimates in Ref. 44, the $1P$ -to- $1S$ relaxation time for this mechanism is around 2 ps in NC's with radii from ~ 2 to ~ 8 nm. This time constant suggests a significantly higher electron relaxation rate than that for the multi-phonon emission, but is somewhat longer than our measured values. This discrepancy may be due to the fact that the calculations of the Auger electron-hole energy transfer rate are sensitive to the hole-phonon coupling, which is not well understood for NC's. An important role of electron-hole interactions in ultrafast energy relaxation is also indicated by recent studies of carrier dynamics in CdSe NC's treated with electron-donating molecules,⁴⁵ for which a dramatic slowing down of electron relaxation is observed upon formation of a complex with charge-separated electrons and holes.

IV. DEPOPULATION DYNAMICS OF ELECTRON QUANTIZED STATES

As was mentioned in the previous section, the interband TA signals are dominated by the electron populations. Therefore, the $1S$ bleaching decay dynamics can be used to evaluate the depopulation rate of the lowest electron quantized state.

In Fig. 9(a) (main frame and inset) we show the $1S$ bleaching time transients for TOPO (crosses) and ZnS (circles) capped NC's with $R=1.17$ nm. To avoid Auger recombination, these data were taken at the low pump level corresponding to excitation of approximately 0.04 $e-h$ pairs per NC on average. For both samples, the decay dynamics are strongly non-exponential. A quantitative analysis of the decay curves was performed using a simple three-exponential fit [lines in Fig. 9(a)]. In the TOPO-capped sample, the $1S$ bleaching decay shows the existence of three

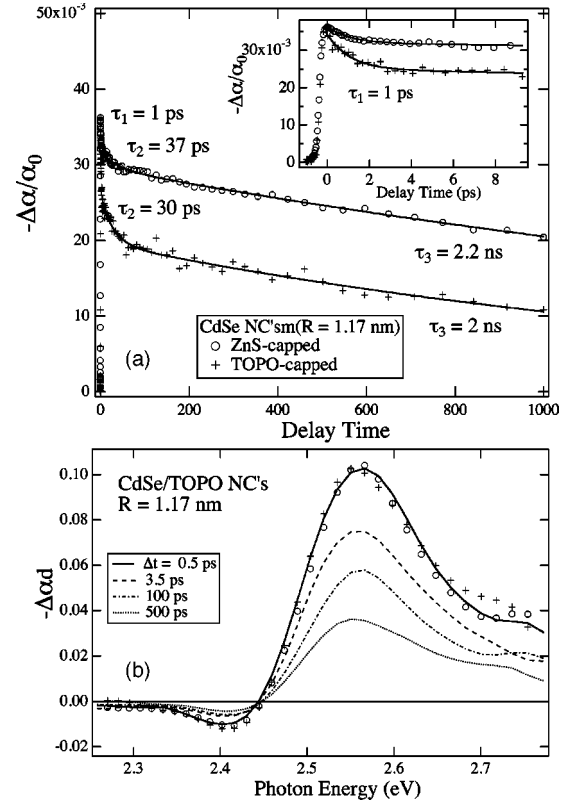


FIG. 9. (a) Nanosecond (main frame) and picosecond (inset) dynamics of the $1S$ -bleaching in ZnS- (circles) and TOPO- (crosses) capped CdSe NC's ($R=1.17$ nm), fit to a three-exponential decay (corresponding relaxation constants are indicated in the figure). (b) TA spectra of TOPO-passivated CdSe NC's ($R = 1.17$ nm) recorded at different delay times between pump and probe pulses (lines). Symbols are 100- (circles) and 500-ps (crosses) spectra scaled to match the 0.5-ps spectrum. The nearly exact match of all three spectra clearly demonstrates that the TA decay is spectrally uniform.

distinct regions. About 35% of the signal amplitude decays very fast with a 1-ps time constant [inset to Fig. 9(a)]. This fast initial stage is followed by a 30-ps decay ($\sim 15\%$ of the signal amplitude), and finally by a slow 2-ns relaxation which accounts for $\sim 50\%$ of the signal amplitude.

An important step in analyzing the relaxation data is to understand whether the observed dynamics are due to relaxation within a single NC (a "single-NC" scenario), or whether they are due to a superposition of dynamics from NC's with different relaxation properties (an "ensemble" scenario), arising, e.g., from size distribution and/or differences in surface passivation. In the absence of Auger recombination, initial 1- and 30-ps decays are too fast to be explained by either radiative or non-radiative $e-h$ recombination back to the ground state. Therefore, the initial fast dynamics are most likely due to electron relaxation from the $1S$ state to a new state (e.g., surface-defect related) in the energy gap. If the fast initial relaxation were characteristic of all NC's ("single-NC" scenario), the electron transition to a new state would have led to either complete relaxation of the $1S$ bleaching or to at least a noticeable change in the TA spectra shape. However, as seen from the spectra in Fig. 9(b), the decay of TA signal is spectrally uniform (the scaled spectra taken at 100 and 500 ps match almost exactly the

spectrum recorded at 0.5 ps), meaning that fast initial ps and final slow ns dynamics originate from different NC's with different relaxation properties. The spectral uniformity of the decay also points towards the fact that the different relaxation behavior is not associated with a size inhomogeneity (which would have led to a shift of the 1S bleaching), but is due to a different number and/or a different type of trapping states dominating the decay in different NC's.

Comparison of 1S bleaching dynamics in samples capped with TOPO and ZnS indicates that the states responsible for a fast initial 1S decay are most likely surface-defect related. Overcoating with an epitaxial layer of ZnS greatly reduces the number of surface defects leading, in particular, to a significant increase in the PL quantum yield³² (from 1.6% to 29% in the case of the samples shown in Fig. 9). The relaxation data also indicate that NC's overcoated with ZnS show an enhancement of the amplitude of the 2-ns TA component which occurs in conjunction with a reduction of the fast ps components. Capping with ZnS almost completely eliminates the 30-ps portion of the TA signal, and suppresses by a factor of 3 the 1-ps component. The fact that 1-ps and 30-ps components are affected by ZnS capping in a different way indicates that they arise from different groups of NC's. Thus, the 1S dynamics observed in the TOPO-capped sample can be interpreted as arising from at least three different groups of NC's with distinctly different relaxation dynamics. We will refer to these groups as to group A, B, and C with relaxation constants 2 ns, 30 ps, and 1 ps, respectively. The increase in the relaxation time in going from group C to group A occurs, presumably, due to improvement in the NC surface passivation. The existence of distinct groups of NC's may be due to the existence of two different types of surface defects acting as efficient electron traps. In group-A NC's, surface passivation eliminates both types of defects and electrons are confined within the NC volume. In group B and C NC's, the degree of surface passivation is decreased, and electron relaxation is dominated by trapping at the particular type of the defect, which is present in a given NC in the greater amount. We will refer to the defects dominating electron relaxation in group B and C NC's as to type B and C defects, respectively.

We also studied the effect of surface-passivation degradation on TA dynamics. In Fig. 10(a), we compare 1S bleaching decay for the 1.73-nm NC's with different degrees of surface passivation. These samples are freshly prepared TOPO-passivated NC's (circles), the same NC's but eight months after preparation (squares), and freshly prepared NC's overcoated with four monolayers of ZnS (crosses). As in the 1.17-nm sample [Fig. 9(a)], the 1S bleaching decay in the 1.73-nm NC's shows three distinct regions: an initial fast 2-ps relaxation, followed by a 40-ps decay and a final 2.6 ns relaxation. In freshly prepared TOPO-capped NC's, the 2- and 40-ps components are respectively $\sim 24\%$ and $\sim 10\%$ of the signal amplitude. Degradation of surface passivation in the aged sample [squares in Fig. 10(a)] has a dramatic effect on the 40-ps component (it increases by almost a factor of 3 upon aging), but does not significantly change the 2-ps component ($\sim 29\%$ in the aged sample). Since TOPO molecules are coordinated to surface metal ions,⁷ the intermediate 40-ps decay is most likely due to trapping at defects associated with metal dangling bonds (B-type defects).

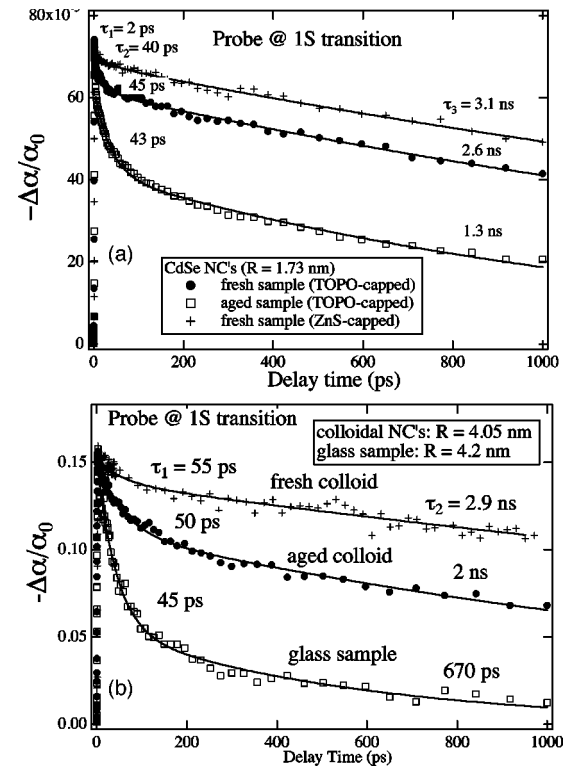


FIG. 10. (a) The 1S-bleaching decay dynamics in small-size CdSe colloidal NC's ($R = 1.73$ nm) with differently prepared surfaces: fresh (circles) and aged (squares) TOPO-capped NC's, and NC's overcoated with ZnS (crosses). Lines are fits to a three-exponential decay. (b) The 1S bleaching decay dynamics in large-size CdSe colloidal NC's with different surface/interface properties. Shown are the data for fresh (crosses) and aged (circles) TOPO-passivated colloidal NC's with $R = 4.05$ nm, and for 4.2-nm NC's dispersed in a glass matrix (squares).

As observed previously for the 1.17-nm samples, overcoating the 1.73-nm NC's with ZnS completely eliminates the 40-ps decay component, and suppresses the 2-ps component by a factor of ~ 1.5 . The suppression of the ps component is less pronounced in this sample than in the ZnS-overcoated 1.17-nm sample, which correlates with its reduced PL quantum yield (12% in the 1.73-nm sample in comparison with 29% in the 1.17-nm sample).

Relaxation data for samples with different types of passivation indicate that the number of C-type defects responsible for the fast 1–2-ps electron decay is nearly unchanged by the degree of TOPO passivation (passivation of metal dangling bonds), but gets reduced upon ZnS capping (improved passivation of both metal and chalcogenide dangling bonds). The nature of these defects is not quite clear. The fact that they are affected by capping of chalcogenide surface ions may be considered as indication of their relation to Se-dangling bonds. On the other hand, bulk-material-based arguments indicate that chalcogenide dangling bonds (metal vacancies) are hole trapping sites.^{19,46} However, the complexity of a NC interface may result in NC-specific Se-based complexes (involving, e.g., surface charges, interaction between Se and Cd surface ions, or interaction with passivating or solvent molecules) which act as electron traps.

The larger NC's ($R > 2.7$ nm) also show a non-exponential decay of the 1S bleaching [Fig. 10(b)]. How-

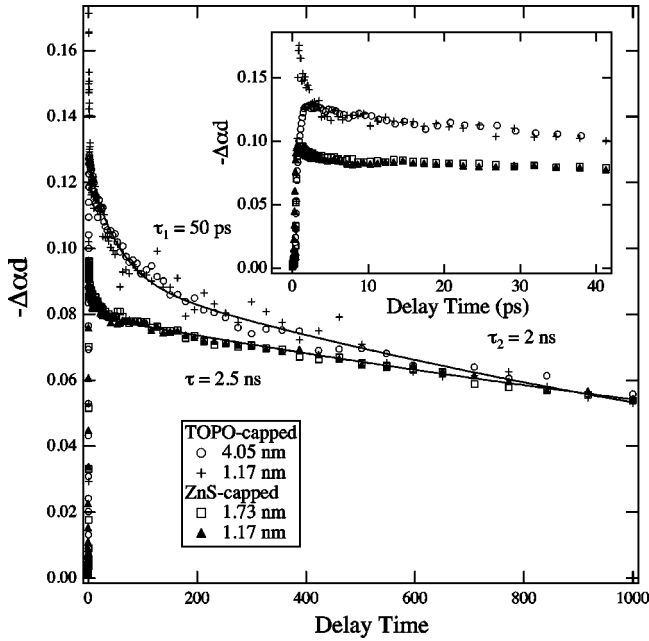


FIG. 11. Nanosecond (main frame) and picosecond (inset) 1S bleaching dynamics for aged TOPO-capped [$R=4.05$ nm (circles) and 1.17 nm (crosses)] and fresh ZnS-capped [$R=1.73$ (squares) and 1.17 (triangles)] CdSe NC's. In the range $\Delta t > 20$ –50 ps, experimental data are fit to either double-exponential (aged samples) or single-exponential (ZnS-overcoated samples) decay.

ever, in contrast to smaller NC's, this decay does not show the initial 1–2-ps component, but rather starts with 50–100-ps relaxation, followed a slow ns decay, indicating the presence of only group A and B NC's. The absence of the fast component may be due to a size-induced transformation of energy spectra modifying the position of the 1S electron level with respect to the C-type defect state. As in the smallest NC's, the amplitude of the sub-100-ps 1S bleaching component in larger NC's increases upon the loss of TOPO passivation during sample aging [compare data shown by circles and crosses in Fig. 10(b)]. A further increase of the sub-100-ps component is observed in NC's grown in a glass matrix by high-temperature precipitation⁴ [squares in Fig. 10(b)]. NC's made by this synthetic route have poorly passivated surfaces, and as a result, in these samples, the 45-ps component due to electron surface trapping dominates the 1S bleaching dynamics.

As already mentioned, aging of colloidal samples leads to degradation of surface passivation and an associated increase of the fast component in the 1S bleaching decay due to enhanced surface trapping. We noticed that the rate of the passivation loss becomes slower upon aging of the samples. After initial relatively fast degradation of passivation, which occurs during the first one or two weeks after preparation, the passivating layer becomes very stable, as indicated by 1S relaxation dynamics which remain unchanged for several months. Interestingly, after the “stabilization” of passivation occurs, all colloids independent of NC size show nearly identical long-term ($\Delta t > 10$ ps) 1S bleaching dynamics. In Fig. 11 (main frame and inset), we compare the 1S dynamics for 4.05- (circles) and 1.17-nm (crosses) TOPO passivated NC's measured 8 months after preparation of the samples. Although the short-term 1S dynamics in these samples are

different (inset to Fig. 11), long-term relaxation behavior for them is remarkably similar. At $\Delta t > 10$ ps, both samples exhibit the 30–50-ps decay, followed by slow 2–3-ns relaxation, with a ratio of the slow to the fast component of ~ 2.5 . For comparison, in the same plot we show normalized dynamics recorded for freshly prepared ZnS-capped 1.17- and 1.73-nm samples. These two time transients closely match each other; both are dominated by the slow 2.5-ns component, with a small portion ($< 20\%$) of the signal relaxing on the ps time scale. The comparison of time transients for TOPO- and ZnS- passivated samples [see also Figs. 9(a) and 10(a)] shows that the long-term 1S dynamics are mostly affected not by NC size, but rather by NC surface properties. The samples with identically poor or good passivations show nearly identical long-term relaxation behavior, independent of NC sizes. The primary effect of NC sizes on carrier dynamics is the appearance of a very fast 1–2-ps component in NC's with radii below ~ 2.5 nm.

V. DEPOPULATION DYNAMICS OF HOLE QUANTIZED STATES

As discussed above, the dynamics of TA bleaching features in the visible spectral range are dominated by electron populations. Therefore, visible TA spectroscopy does not allow one to clearly observe hole dynamics. In Ref. 47, in addition to fs TA spectroscopy we applied a complementary technique of time-resolved fs PL up-conversion to separate electron and hole relaxation paths in CdS NC/glass samples. In contrast to state-filling-induced bleaching, which is proportional to the sum of the electron and hole occupation numbers, PL is proportional to the product of these numbers; therefore PL dynamics are dominated by the carriers with the shortest relaxation time. In CdS samples ($R \approx 4$ nm) studied in Ref. 47, the 1S bleaching decay was dominated by a slow component with a 55-ps time constant, due to depopulation of the 1S electron state. The PL relaxation occurred on a much shorter (~ 1 ps) time scale, indicative of fast hole relaxation, which was tentatively assigned to trapping at chalcogenide surface dangling bonds.^{19,47}

In the present paper, to study hole relaxation dynamics we use fs IR spectroscopy of intra-band transitions. Due to the difference in energies of electron and hole intra-band transitions, the use of a fs IR probe allows the spectral separation of electron and hole TA signals. In Fig. 12 (main frame), we show a series of time scans taken for the 1.73-nm sample at different IR spectral energies (from 0.5 to 0.65 eV) (lines) in comparison to the 1S dynamics (circles). Both electron and hole intraband absorptions contribute to the IR signals at each energy. At $\Delta t > 50$ ps, the IR TA dynamics closely match those of the 1S bleaching, indicating that the long-lived portion of the IR signal is due to electron intra-band absorption. This leads us to assign the short-lived IR TA component to holes. In the near-IR spectral range studied, the intra-band electron signal is due to the 1S-1P transition. For the 1.73-nm sample, the energy of this transition is ~ 0.45 eV.⁴⁸ For a ~ 0.1 eV transition broadening (estimated for a $\sim 5\%$ size dispersion), the 1S-1P electron intra-band absorption is expected to drop significantly at spectral energies above 0.55 eV. This is consistent with the observed reduction of the long-lived TA IR component at higher spec-

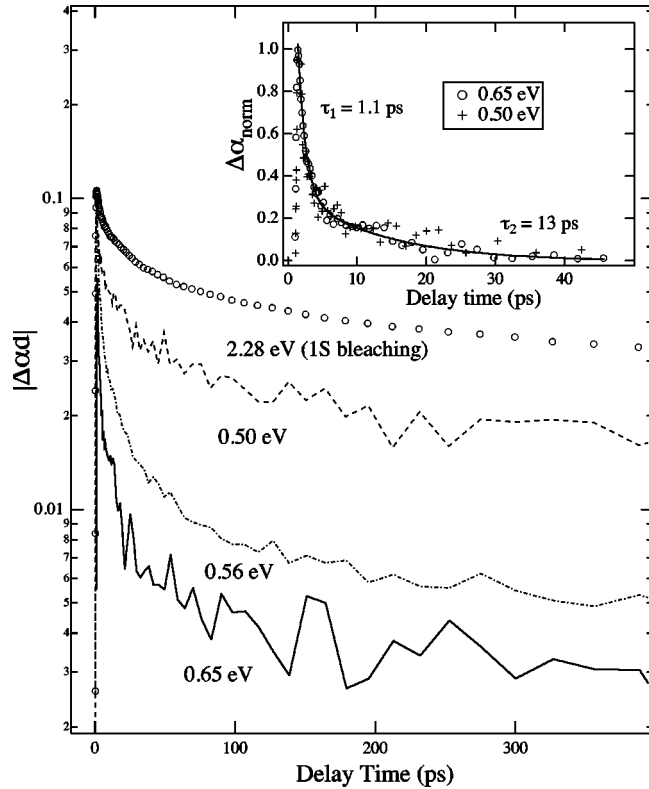


FIG. 12. Near-IR TA dynamics at different spectral energies (lines) in comparison to the 1S bleaching decay (circles). Inset: The fast hole-related component in the near-IR TA derived by subtracting the scaled 1S bleaching dynamics from the near-IR time transients [shown are the data for two spectral energies: 0.65 eV (circles) and 0.50 eV (crosses)].

tral energies. As a result of this reduction, at $\hbar\omega > 0.55$ eV, the IR signals are dominated by the short-lived hole intraband absorption. To extract the hole relaxation dynamics, we have subtracted the normalized 1S bleaching signal (1S time transients were scaled to match the long-lived portion of the IR signal) from the IR TA time transients. The extracted dynamics (see inset to Fig. 12) are independent of the IR spectral energy, indicating that the IR TA can be indeed understood as a superposition of two spectrally-independent dynamics (due to electron and hole relaxation) with spectrally-dependent weighting factors. The extracted hole signals are extremely fast, with nearly 90% of the signal amplitude decaying on the 1-ps time scale. A similar fast relaxation of the hole intraband absorption is observed in other colloidal and glass samples with sizes from ~ 1 –4 nm. The typical range of time constants for the hole relaxation process is from 0.7 to 2 ps [see Fig. 13(a)].

The sub-ps decay of the hole-related portion of the TA is indicative of extremely fast depopulation of hole quantized states. Analysis of the 1S bleaching decay performed in section IV shows that the rate of depopulation of the 1S electron state is very sensitive to NC surface properties. In contrast, the hole dynamics are practically unaffected by NC surface passivation, as clearly seen from comparison of the IR traces for samples with different surface properties. In Fig. 13(b) we show near-IR dynamics for the 1.73-nm freshly prepared and aged TOPO-capped samples, and freshly prepared ZnS-capped sample [visible dynamics for the same set of samples

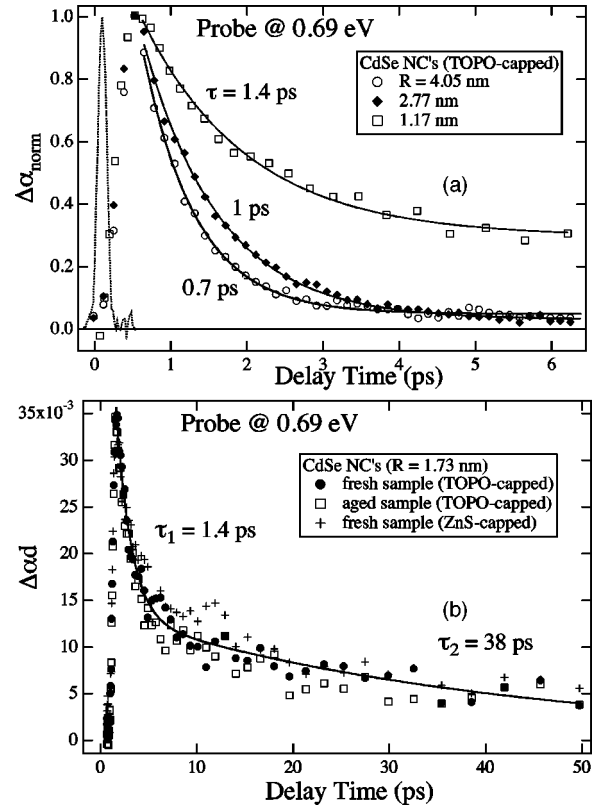


FIG. 13. (a) Near-IR TA dynamics at 0.69 eV for TOPO-capped CdSe NC's [$R=4.05$ (circles), 2.77 (diamonds), and 1.17 nm (squares)] fit to a single-exponential decay. (b) Near-IR TA dynamics at 0.69 eV for CdSe colloidal NC's ($R=1.73$ nm) with differently prepared surfaces: fresh (circles) and aged (squares) TOPO-capped samples, and fresh ZnS-capped sample (crosses)].

are shown in Fig. 10(a)]. In contrast to the pronounced differences in 1S bleaching decay [Fig. 10(a)], the near-IR TA dynamics are essentially identical in all three samples and are characterized by an extremely fast time constant of 1.4 ps. The fact that the hole dynamics are extremely fast in all types of samples, including ZnS-overcoated NC's, indicates that these dynamics are not due to trapping at localized surface defects, but rather are due to relaxation into intrinsic NC states (e.g., hole self-trapped surface states as analyzed in Ref. 49) or intrinsically unpassivated interface states. The importance of hole surface trapping (localization) in II-VI NC's has been also indicated by several previous experimental studies.^{19,48,50}

VI. CONCLUSIONS

We have performed fs studies of intra-band energy relaxation in CdSe NC's with radii in the ~ 1 –4 nm range. We observe a fast sub-ps 1P-to-1S electron relaxation with a rate exceeding by up to an order of magnitude that for unscreened electron-LO-phonon interaction in bulk materials. The relaxation rate is enhanced in NC's of smaller radius, reaching 6 eV ps⁻¹ in samples with $R \approx 1.2$ nm. These observations directly contradict predictions for a phonon bottleneck, and demonstrate the importance of non-phonon relaxation channels which likely involve Auger-type electron-hole energy transfer.

To distinguish between the depopulation dynamics of electron and hole quantized states, we use fs IR TA which allows us to probe electron and hole intraband transitions. We observe extremely fast relaxation of hole intraband signals, indicating depopulation of hole quantized states on sub-ps-to-ps time scales in all types of samples, independent of NC surface properties. This strongly suggests that the hole trapping sites are not defect-related but rather are intrinsic to nanocrystal quantum dots.

We observe that the electron decay is strongly non-exponential, and can be split into three distinct regions: an initial 1–2-ps relaxation, an intermediate sub-100-ps decay, and a final slow 2–3-ns relaxation. We explain this multi-component relaxation behavior as arising from the superposition of dynamics from NC's with different rates of relax-

ation (“ensemble” effect), caused by the presence of two different types of electron surface traps (surface defects). In contrast to the strong sensitivity to NC surface properties, electron relaxation is almost unaffected by NC sizes. The most pronounced size-dependent effect is a disappearance of the initial fast 1–2-ps relaxation component in NC's with sizes greater than ~ 2.5 nm.

ACKNOWLEDGMENTS

This research was supported by the Los Alamos Directed Research and Development Funds, under the auspices of the U.S. Department of Energy. C.A.L. and M.G.B. also acknowledge partial funding from the NSF-MRSEC program under Grant No. DMR-9400334.

*Electronic address: klimov@lanl.gov

- ¹A. L. Efros and A. Efros, *Sov. Phys. Semicond.* **16**, 772 (1982).
- ²L. Brus, *J. Chem. Phys.* **80**, 4473 (1984).
- ³H. Asahi, *Adv. Mater.* **9**, 1019 (1997).
- ⁴A. Ekimov, *J. Lumin.* **70**, 1 (1996).
- ⁵N. Borrelli, D. Hall, H. Holland, and D. Smith, *J. Appl. Phys.* **61**, 5399 (1987).
- ⁶L. Brus, *Appl. Phys. A: Solids Surf.* **53**, 465 (1991).
- ⁷C. Murray, D. Norris, and M. Bawendi, *J. Am. Chem. Soc.* **115**, 8706 (1993).
- ⁸S. Majetich and A. Carter, *J. Phys. Chem.* **97**, 8727 (1993).
- ⁹A. Kortan, R. Hull, R. Opila, M. Bawendi, M. Steigerwald, P. Carroll, and L. E. Brus, *J. Am. Chem. Soc.* **112**, 1327 (1990).
- ¹⁰G. Counio, S. Esnouf, T. Gacoin, and J. Boilot, *J. Phys. Chem.* **100**, 20021 (1996).
- ¹¹N. Greenham, X. Peng, and A. Alivisatos, *Phys. Rev. B* **54**, 17 628 (1996).
- ¹²C. Murray, C. Kagan, and M. Bawendi, *Science* **270**, 1335 (1995).
- ¹³E. Conwell, *High Field Transport in Semiconductors* (Academic Press, New York, 1967).
- ¹⁴S. Prabhu, A. Vengurlekar, and J. Shah, *Phys. Rev. B* **51**, 14 233 (1995).
- ¹⁵V. Klimov, P. Haring Bolivar, and H. Kurz, *Phys. Rev. B* **52**, 4728 (1995).
- ¹⁶U. Bockelmann and G. Bastard, *Phys. Rev. B* **42**, 8947 (1990).
- ¹⁷H. Benisty, C. Sotomayor-Torres, and C. Weisbuch, *Phys. Rev. B* **44**, 10 945 (1991).
- ¹⁸T. Inoshita and H. Sasaki, *Phys. Rev. B* **46**, 7260 (1992).
- ¹⁹V. Klimov, P. Haring Bolivar, and H. Kurz, *Phys. Rev. B* **53**, 1463 (1996).
- ²⁰U. Woggon, H. Giessen, F. Gindele, O. Wind, B. Fluegel, and N. Peyghambarian, *Phys. Rev. B* **54**, 17 681 (1996).
- ²¹V. Klimov, S. Hunsche, and H. Kurz, *Phys. Rev. B* **50**, 8110 (1994).
- ²²K. Shum, W. B. Wang, R. Alfano, and K. Jones, *Phys. Rev. Lett.* **68**, 3904 (1992).
- ²³V. Klimov and D. McBranch, *Phys. Rev. Lett.* **80**, 4028 (1998).
- ²⁴T. S. Sosnowskii, T. Norris, H. Jiang, J. Singh, K. Kamat, and P. Bhattacharya, *Phys. Rev. B* **57**, 9423 (1998).
- ²⁵A. L. Efros, *Phys. Rev. B* **46**, 7448 (1992).
- ²⁶M. C. Nuss, W. Zinth, and W. Kaiser, *Appl. Phys. Lett.* **49**, 1717 (1986).
- ²⁷M. Ghanassi, M. Schanne-Klein, F. Hache, A. Ekimov, and D. Ricard, *Appl. Phys. Lett.* **62**, 78 (1993).
- ²⁸V. Klimov and D. McBranch, *Phys. Rev. B* **55**, 13 173 (1997).
- ²⁹R. Shoenlein, D. Mittleman, J. Shiang, A. Alivisatos, and C. Shank, *Phys. Rev. Lett.* **70**, 1014 (1993).
- ³⁰D. Mittleman, R. Shoenlein, J. Shiang, V. L. Colvin, A. Alivisatos, and C. Shank, *Phys. Rev. B* **49**, 14 435 (1994).
- ³¹V. Klimov and D. McBranch, *Opt. Lett.* **23**, 277 (1998).
- ³²M. Hines and P. Guyot-Sionnest, *J. Phys. Chem.* **100**, 468 (1996).
- ³³D. Ricard, M. Ghanassi, and M. Schanneklein, *Opt. Commun.* **108**, 311 (1994).
- ³⁴D. Norris and M. Bawendi, *Phys. Rev. B* **53**, 16 338 (1996).
- ³⁵A. I. Ekimov, F. Hache, M. C. Schanne-Klein, D. Ricard, C. Flytzanis, I. A. Kudryavtsev, T. V. Yazeva, A. V. Rodina, and A. L. Efros, *J. Opt. Soc. Am. B* **10**, 100 (1993).
- ³⁶Y. Z. Hu, S. W. Koch, and D. B. T. Thoai, *Mod. Phys. Lett. B* **4**, 1009 (1990).
- ³⁷K. Kang, A. Kepner, S. Gaponenko, S. Koch, Y. Hu, and N. Peyghambarian, *Phys. Rev. B* **48**, 15 449 (1993).
- ³⁸D. Norris, A. Sacra, C. Murray, and M. Bawendi, *Phys. Rev. Lett.* **72**, 2612 (1994).
- ³⁹S. Hunsche, T. Dekorsy, V. Klimov, and H. Kurz, *Appl. Phys. B: Lasers Opt.* **62**, 3 (1996).
- ⁴⁰E. Yoffa, *Phys. Rev. B* **23**, 1909 (1981).
- ⁴¹P. Kocevar, *Physica B* **134**, 155 (1985).
- ⁴²P. Sercel, *Phys. Rev. B* **51**, 14 532 (1995).
- ⁴³U. Bockelmann and T. Egler, *Phys. Rev. B* **46**, 15 574 (1992).
- ⁴⁴A. L. Efros, V. A. Kharchenko, and M. Rosen, *Solid State Commun.* **93**, 281 (1995).
- ⁴⁵P. Guyot-Sionnest, M. Shim, C. Matranga, and M. Hines, *Phys. Rev. B* **60**, R2181 (1999).
- ⁴⁶N. Chestnoy, T. Harris, R. Hull, and L. Brus, *J. Phys. Chem.* **90**, 3393 (1986).
- ⁴⁷V. Klimov, P. Haring Bolivar, H. Kurz, and V. Karavanskii, *Superlattices Microstruct.* **20**, 395 (1996).
- ⁴⁸P. Guyot-Sionnest and M. Hines, *Appl. Phys. Lett.* **72**, 686 (1998).
- ⁴⁹L. Banyai, P. Gilliot, Y. Z. Hu, and S. W. Koch, *Phys. Rev. B* **45**, 14 136 (1992).
- ⁵⁰M. Bawendi, W. Wilson, L. Rothberg, P. Carroll, T. Jedju, M. Steigerwald, and L. Brus, *Phys. Rev. Lett.* **65**, 1623 (1990).